Available online at www.sciencedirect.com

ScienceDirect

Ceramics International 37 (2011) 593–598

CERAMICS
INTERNATIONAL

www.elsevier.com/locate/ceramint

Growth of Sb_2O_3 submicron rods by the thermal evaporation of a mixture of Zn and Sb powders

Hyoun Woo Kim *, Hyo Sung Kim, Han Gil Na, Ju Chan Yang,
Mesfin Abayneh Kebede, Chongmu Lee

Division of Materials Science and Engineering, Inha University, Incheon 402-751, Republic of Korea

Received 20 February 2010; received in revised form 28 February 2010; accepted 27 September 2010
Available online 31 October 2010

Abstract

We synthesized crystalline Sb_2O_3 rods by heating a mixture of Sb and Zn powders. Scanning electron microscopy indicated that the Zn powder as well as the growth temperature affected the morphology of the product. We discussed the possible growth mechanisms. Scanning electron microscopy, X-ray diffraction, selected area electron diffraction, Raman spectroscopy and transmission electron microscopy collectively revealed that the products consisted of Sb_2O_3 having a pure cubic structure with diameters in the range of 150–600 nm. The photoluminescence spectrum of the Sb_2O_3 submicron rods under excitation at 325 nm exhibited a visible light emission.

Keywords: Submicron rods; Sb_2O_3; Thermal evaporation

1. Introduction

Low-dimensional materials, such as rods, belts, wires and particles, have potential applications in nanoelectronics and optoelectronics, due to their novel physical and chemical properties. Particularly, submicron rods or wires have peculiar properties, such as the finite-size effect of flux pinning in superconducting wires [1], enhanced field emission behavior [2], quantum Hall effect [3], and excellent magnetic properties including a high coercive (magnetic) field [4], suppression of spin relaxation [5] and charge–density–wave current conversion [6].

Antimony trioxide (Sb_2O_3) is an important semiconducting material, which has been widely used as a fire retardant in membranes in the plastic industry, as enclosures of electric devices, and as a catalytic agent in organic synthesis [7–15]. Sb_2O_3 is not only an interesting semiconducting material with unique optical and optoelectronic properties [16], but also has remarkable magnetic properties [17–20]. Accordingly, Sb_2O_3 submicron rods with their excellent physical and chemical properties have potential applications in future advanced optoelectronic and magnetic devices.

Up to the present, researchers have fabricated one-dimensional (1D) structures of Sb_2O_3 by various methods, including the air oxidation of Sb metal in a mixed solution made of ethylenediamine (EDA) and deionized water (DIW) [16], the microemulsion method [21], the hydrothermal route [22], the carbon nanotube (CNT)-template technique [23], and the transformation of nanoporous oxoselenoantimonates [24]. In particular, Ye et al. successfully synthesized 1D structures of Sb_2O_3 by the thermal heating of Sb_2S_3 [25], which is simple and suitable for the established ULSI fabrication process. However, in their work, the products consisted of a variety of morphologies, such as fibers and tubules [25]. In the present study, we heated a mixture of Sb and Zn powders, leading to the production of Sb_2O_3 submicron rods, which have a homogeneous rectangular cross-section. It was observed that not only the substrate temperature, but also the addition of Zn affected the generation of the thin rods. In addition, we investigated the structural and photoluminescence (PL) properties of the as-prepared Sb_2O_3 rods.

2. Experimental

In this study, we employed Au-coated Si substrates, which were fabricated using Si as the starting material onto which an

---

* Corresponding author. Tel.: +82 32 860 7544; fax: +82 32 862 5546.
E-mail address: hwkim@inha.ac.kr (H.W. Kim).

0272-8842/$36.00 © 2010 Elsevier Ltd and Techna Group S.r.l. All rights reserved.
doi:10.1016/j.ceramint.2010.09.050

Au layer with a thickness of about 3 nm was deposited by ion sputtering (Emitech, K757X). The synthesis process was carried out in a quartz tube. Zn metal powders and Sb nanopowders, which were fully mixed with a weight ratio of 1:1 (approximately 2 g in total), were used as the source material. The source material and substrate were placed on the lower and upper holders, respectively, in the center of a quartz tube inserted into a vertical furnace. The vertical distance between the powders and substrate was approximately 10 mm, with the Au-coated side facing downwards. During the experiment, the furnace was maintained at a temperature in the range of 700–800 °C with the ambient gas ($Ar + O_2$) being at a constant total flow rate of 2 standard liters per min (slm). After 1 h of evaporation, the furnace was allowed to cool down to room temperature.

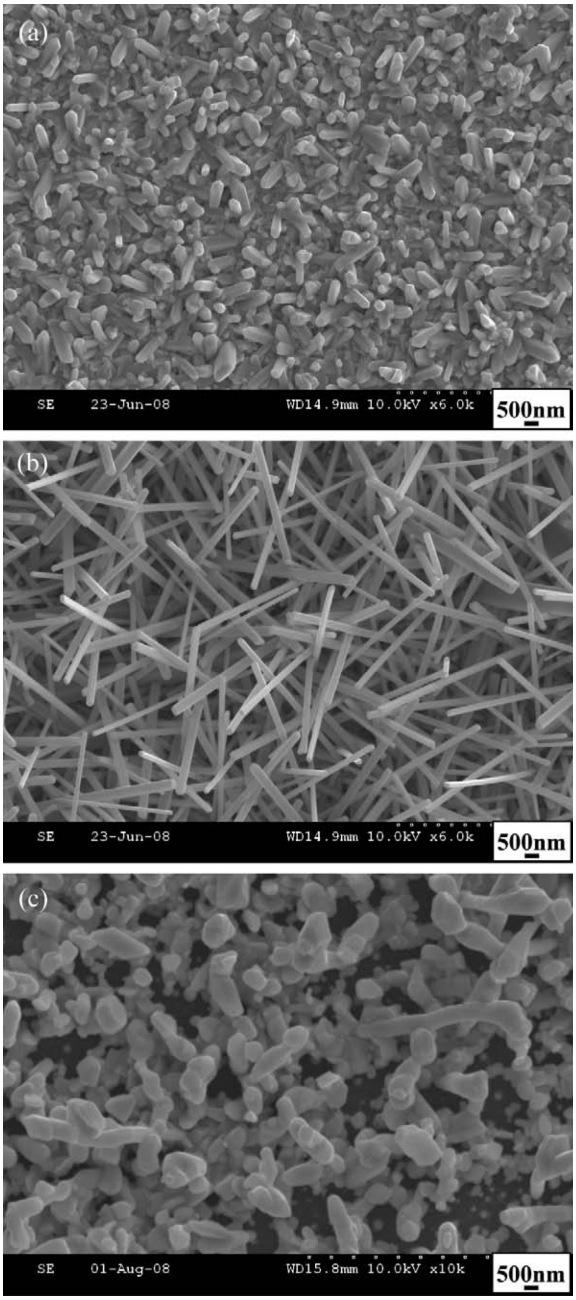

Fig. 1. Top-view SEM images of the products with an evaporation temperature of: (a) 700, (b) 750, and (c) 800 °C.

The crystal structure of the products was investigated by X-ray diffraction (XRD, X'pert MRD-Philips) with $CuK\alpha_1$ radiation and an incidence angle of 0.5°. Scanning electron microscopy (SEM) was carried out using a Hitachi S-4200 scanning electron field emission microscope. A Philips CM-200 microscope was used for the transmission electron microscopy (TEM), energy-dispersive X-ray spectroscopy (EDX), and selected area electron diffraction (SAED) analyses. PL measurements were performed using a He–Cd laser line (325 nm, 55 mW) as the excitation source at room temperature. Micro-Raman spectra were taken at room temperature in the spectral range of 100–600 cm^{-1} using a Renishaw Raman spectromicroscope in the open air. A He–Ne laser beam with a wavelength of 633 nm was used for Raman excitation.

3. Results and discussion

Fig. 1(a–c) shows the SEM images of the final products obtained with evaporation temperatures of 700, 750, and 800 °C, respectively. It is evident that the products grown at 750 °C comprise thin 1D rods, whereas those grown at both 700 and 800 °C contain cluster-like or thick 1D structures. It is noteworthy that the rods grown at 750 °C have a diameter in the range of 150–600 nm. Fig. 2 shows the XRD spectrum of the product grown at 750 °C. The diffraction peaks in the XRD spectrum can be indexed to the cubic structure of Sb_2O_3 (JCPDS 72-1854).

Fig. 3(a and b) shows the images of the elemental maps in regard to Sb and O elements, respectively. It is observed that the rod comprises Sb and O elements. Fig. 3(c) is a high resolution TEM (HRTEM) image enlarging an area near the surface of a rod. The interplanar spacings are about 0.23 and 0.27 nm, which correspond to the (4 2 2) and (4 4 0) planes of cubic Sb_2O_3, respectively. Fig. 3(d) shows the associated SAED pattern, revealing that the rod has a single crystalline structure.

Fig. 4 shows the Raman spectrum of the Sb_2O_3 rods, in which the peak at 521 cm^{-1} was identified as the TO phonon mode in the silicon (Si) crystal structure [26], presumably from

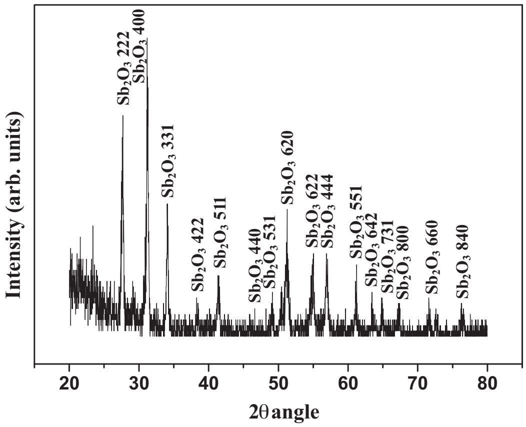

Fig. 2. XRD patterns recorded from the product with an evaporation temperature of 750 °C.

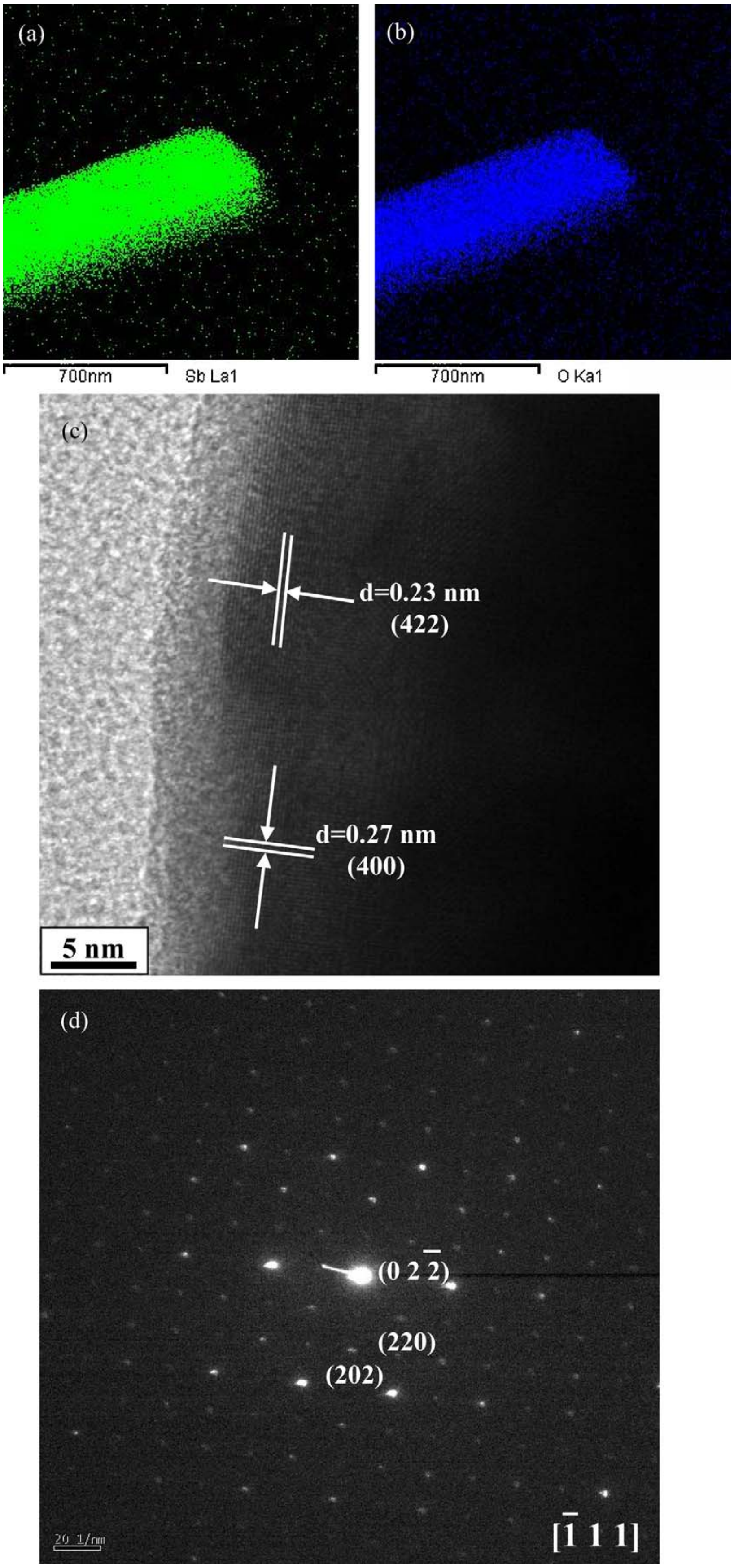

Fig. 3. TEM–EDX elemental maps of: (a) Sb and (b) O elements. (c) Lattice-resolved TEM image near the surface of a rod. (d) Corresponding SAED pattern.

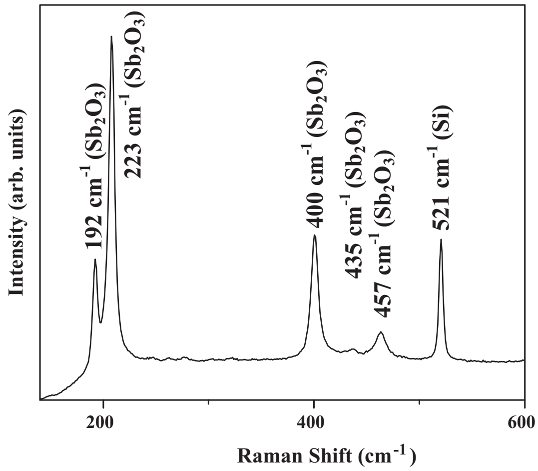

Fig. 4. Room-temperature Raman spectrum of the product with an evaporation temperature of 750 °C.

the Si substrates. Also, the peak at around 192 cm^{-1} is usually observed from bulk Sb_2O_3 [27–29]. The peaks at around 400 cm^{-1} and 457 cm^{-1} are similar to the ones observed from micro-sized Sb_2O_3 octahedra [30]. On the other hand, the peaks at 223 cm^{-1} and 435 cm^{-1} have been previously reported from the Raman spectra of single-crystalline Sb_2O_3 nanowires [31].

Since the SEM and TEM analyses provided no evidence for the presence of the catalyst at the tips of the 1D structures (Figs. 1(b) and 3(a and b)), the growth mechanism of the Sb_2O_3 rods cannot be ascribed to the tip-growth VLS mechanism. The reaction that occurred in the formation of the Sb_2O_3 crystal nucleus may be illustrated as follows: $4Sb + 3O_2 \rightarrow 2Sb_2O_3$ [31]. The Sb-associated vapors from the Sb powders would react with O_2 in the ambient gas to generate solid Sb_2O_3 nuclei on the substrate. It is surmised that the Au nanoparticles or islands, which are generated from the Au-coated Si substrates during the heating process, may stay at the bottom of the rods during the growth process. In a previous work, the growth of the CNTs was attributed to the base growth mechanism, in which the metal catalyst remains at the bottom of the nanostructures [32]. Fig. 5(a) shows an enlarged SEM image of the Sb_2O_3 rods obtained with an evaporation temperature of 750 °C. It is observed that the tip parts of the submicron rods mostly have a rectangular shape, which presumably originates from the cubic structure of Sb_2O_3.

On the other hand, Fig. 5(b) shows a SEM image of the final product obtained by heating the Sb powders at 750 °C without any Zn powder. By comparing Fig. 5(b) with Fig. 1(b)/Fig. 5(a), we noticed that the rods became thinner when the Zn powders were added, implying that the Zn powders play a role in the growth of the submicron rods. From the Sb-Zn binary phase diagram, we would expect the melting point to be decreased by the addition of Zn [33]. Accordingly, we surmise that the addition of Zn induces less supercooling and, thus, the secondary growth from the stem rods is suppressed. Instead, relatively thin 1D structures will be favored. On the contrary, the presence of less Zn leads to severe supercooling, facilitating the growth of secondary branches or clusters on the surface of the stem rods and ultimately generating thicker 1D structures.

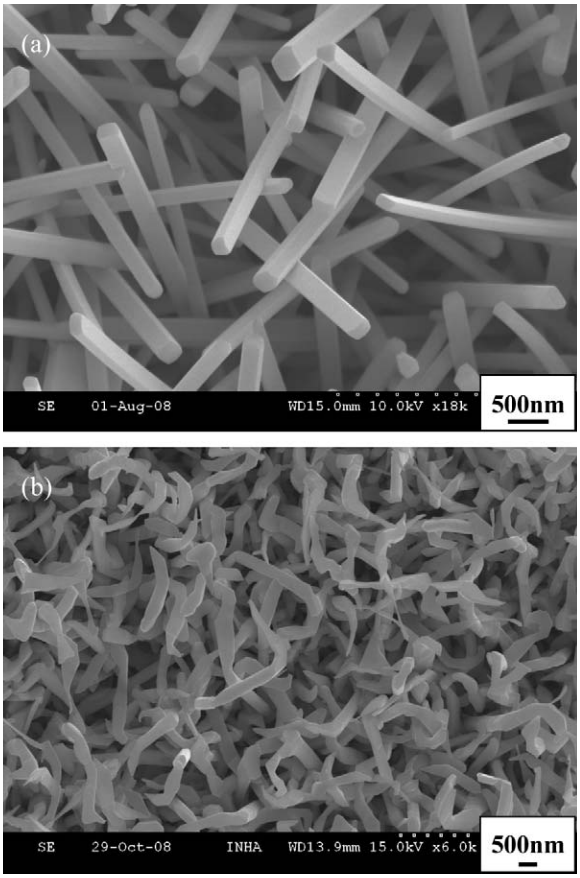

Fig. 5. (a) Enlarged SEM image of the products with an evaporation temperature of 750 °C, in which a mixture of Sb and Zn powders were heated. (b) Top-view SEM image of the products with an evaporation temperature of 750 °C, in which Sb powders were heated without Zn powers.

In addition, it is possible that the addition of Zn reduces the activity of Sb in Sb–Zn binary alloy, which brings about the reduction of Sb partial pressure and thus the slowing down of the formation of the Sb_2O_3 crystal. The slower reaction is supposed to be closer to the equilibrium process, favoring the growth of thin 1D structures.

Fig. 1 clearly indicates that the change of growth temperature contributes to the variation in the morphology of Sb_2O_3 structures: it affects the surface diffusion, desorption, and re-evaporation of the adsorbed vapor species, as well as the amount of reactive vapor generated [34]. At the lower temperature (700 °C) (Fig. 1(a)), insufficient thermal energy of the Sb vapor allows the atoms to be deposited exactly where they land with low surface diffusion, generating a rough film with cluster-like structures [35]. By comparing Fig. 1(c) with Fig. 1(b), we observe that the rods grown at 800 °C are noticeably thicker and shorter than those grown at 750 °C. At higher temperature, the sufficiently high thermal energy allows for a high rate of desorption, re-evaporation, and redeposition. Accordingly, thick and short rods, instead of thin and long ones, have been produced at 800 °C [35].

Fig. 6 shows the PL spectrum of the Sb_2O_3 rods. It shows a broad band with a peak wavelength of around 470 nm. The broad blue emission profile between 390 and 500 nm was attributed to emissions related to defects such as oxygen

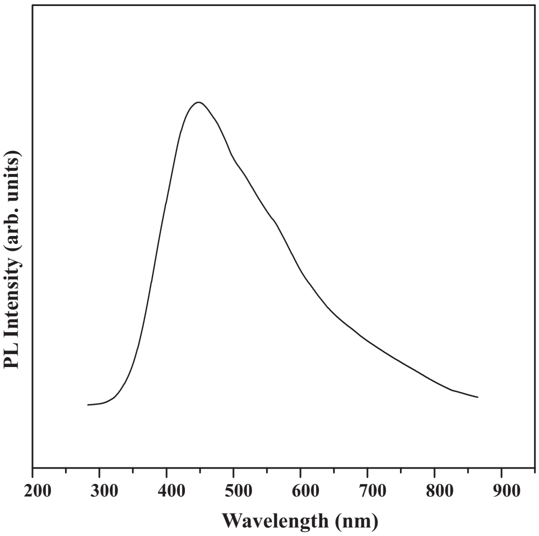

Fig. 6. Room-temperature PL spectrum of Sb_2O_3 rods with an excitation wavelength at 325 nm.

vacancies [33]. It is shown that the overall PL intensity was not dependent on the growth temperature (see Supplementary material S-1). At higher temperatures, the oxygen vacancy concentration in the nanowire tends to increase. On the other hand, the increase of the oxygen pressure in the ambient will suppress the increase of the oxygen vacancy concentration in the nanowire. This will result in the insignificant change of oxygen vacancy concentration and thus the invariance of PL intensity with varying the growth temperature.

4. Conclusion

We fabricated Sb_2O_3 rods via a thermal evaporation method, which consisted of heating a mixture of Sb and Zn powders. The addition of Zn powders as well as the optimal substrate temperature was required for the growth of thin rods. Possible associated growth mechanisms were suggested. The XRD, TEM and SAED analyses collectively indicated that the product is crystalline with a cubic Sb_2O_3 structure. Also, the Raman spectrum of the submicron rods exhibits the characteristics of the Sb_2O_3 structure. The PL measurement shows a visible light emission band, which holds promise for future optoelectronic applications.

Acknowledgements

This research was supported by National Nuclear R&D Program through the National Research Foundation of Korea (NRF) funded by the Ministry of Education, Science and Technology (2010-0018699).

Appendix A. Supplementary data

Supplementary data associated with this article can be found, in the online version, at doi:10.1016/j.ceramint.2010.09.050.

References

[1] X.S. Ling, J.D. McCambridge, D.E. Prober, L.R. Motowidlo, B.A. Zeitlin, M.S. Walker, Flux dynamics in submicron superconducting NbTi wires, Physica B 194–196 (1994) 1867–1868.

[2] N.S. Ramgir, D.J. Late, A.B. Bhise, M.A. More, I.S. Mulla, D.S. Joag, K. Vijayamohanan, ZnO multipods, submicron wires, and spherical structures and their unique emission behavior, J. Phys. Chem. B 110 (2006) 18236–18242.

[3] J. Wrobel, J. Jaroszynski, T. Dietl, K. Reginski, M. Bugajski, Conductance noise of submicron wires in the regime of quantum Hall effect, Physica B 256–258 (1998) 69–73.

[4] J.I. Martin, J.L. Costa-Kramer, F. Briones, J.L. Vicent, Fabrication and magnetic properties of long Ni wires of submicron width, J. Magn. Magn. Mater. 221 (2000) 215–218.

[5] A.W. Holleitner, V. Sih, R.C. Myers, A.C. Gossard, D.D. Awschalom, Suppression of spin relaxation in submicron InGaAs wires, Phys. Rev. Lett. 97 (2006) 036805–036809.

[6] O.C. Mantel, F. Chalin, C. Dekker, H.S.J. van der Zant, Y.I. Latyshev, B. Pannetier, P. Monceau, Charge–density–wave current conversion in submicron $NbSe_3$ wires, Phys. Rev. Lett. 84 (2000) 538–541.

[7] N. Chand, S. Verma, Surface and strength properties of PVC–Sb_2O_3 flame retardant coated sunhemp fiber, J. Fire Sci. 9 (1991) 251–258.

[8] H. Sato, K. Kondo, S. Tsuge, H. Ohtani, N. Sato, Mechanisms of thermal degradation of a polyester flame-retarded with antimony oxide/brominated polycarbonate studied by temperature-programmed analytical pyrolysis, Polym. Degrad. Stabil. 62 (1998) 41–48.

[9] M. Longerey, J.M. Cuesta, P. Gaudon, A. Crespy, Talcs and brominated trimethylphenyl indane/Sb_2O_3 blend in a PP–PE copolymer, Polym. Degrad. Stabil. 64 (1999) 489–496.

[10] J. Spengler, F. Anderle, E. Bosch, R.K. Grasselli, B. Pillep, P. Behrens, O.B. Lapina, A.A. Shubin, H.J. Eberle, H. Knozinger, Antimony oxide-modified vanadia-based catalysts – physical characterization and catalytic properties, J. Phys. Chem. B 105 (2001) 10772–10783.

[11] H.C. Liu, H. Imoto, T. Shido, Y. Iwasawa, Selective ammoxidation of isobutylene to methacrylonitrile on a new family of crystalline Re–Sb–O catalysts, J. Catal. 200 (2001) 69–78.

[12] B. Duh, Effect of antimony catalyst on solid-state polycondensation of poly(ethylene terephthalate), Polymer 43 (2002) 3147–3154.

[13] H.H. Liu, Y. Iwasawa, Unique Performance and characterization of a crystalline $SbRe_2O_6$ catalyst for selective ammoxidation of Isobutane, J. Phys. Chem. B 106 (2002) 2319–2329.

[14] B. Pillep, P. Behrens, U.-A. Schubert, J. Spengler, H. Knözinger, Mechanical and thermal spreading of antimony oxides on the TiO_2 surface: dispersion and properties of surface antimony oxide species, J. Phys. Chem. B 103 (1999) 9595–9603.

[15] U.-A. Schubert, F. Anderle, J. Spengler, J. Zühlke, H.-J. Eberle, R.K. Grasselli, H. Knözinger, Possible effects of site isolation in antimony oxide-modified vanadia/titania catalysts for selective oxidation of o-xylene, Top. Catal. 15 (2001) 195–200.

[16] Z. Deng, F. Tang, D. Chen, X. Meng, L. Cao, B. Zou, A simple solution route to single-crystalline Sb_2O_3 nanowires with rectangular cross sections, J. Phys. Chem. B 110 (2006) 18225–18230.

[17] P. Brahma, A.K. Giri, D. Chakravorty, M. Tiwari, D. Bahadur, Magnetic properties of Sb_2O_3-doped Ba–M hexagonal ferrites, J. Magn. Magn. Mater. 102 (1991) 109–115.

[18] B.V. Raghavaiah, D. Krishna Rao, N. Veeraiah, Magnetic properties of PbO–Sb_2O_3–As_2O_3 glasses containing iron ions, J. Magn. Magn. Mater. 284 (2004) 363–368.

[19] M.S. Reddy, G.M. Krishna, N. Veeraiah, Spectroscopic and magnetic studies of manganese ions in ZnO–Sb_2O_3–B_2O_3 glass system, J. Phys. Chem. Solids 67 (2006) 789–795.

[20] G.K. Semin, A.A. Boguslavsky, NQR determination of local magnetic fields in senarmonite (Sb_2O_3), Chem. Phys. Lett. 251 (1996) 250–251.

[21] L. Guo, Z. Wu, T. Liu, W. Wang, H. Zhu, Synthesis of novel Sb_2O_3 and Sb_2O_5 nanorods, Chem. Phys. Lett. 318 (2000) 49–52.

[22] X. Chen, X. Wang, C. An, J. Liu, Y. Qian, Synthesis of Sb_2O_3 nanorods under hydrothermal conditions, Mater. Res. Bull. 40 (2005) 469–474.

[23] S. Friedrichs, R.R. Meyer, J. Sloan, A.I. Kirkland, J.L. Hutchinson, M.L.H. Green, Complete characterisation of a Sb_2O_3/(21,8)SWNT inclusion composite, Chem. Commun. 2001 (2001) 929–930.

[24] D. Sendor, T. Weirich, U. Simon, Transformation of nanoporous oxoselenoantimonates into Sb_2O_3-nanoribbons and nanorods, Chem. Commun. 2005 (2005) 5790–5792.

[25] C. Ye, G. Meng, L. Zhang, G. Wang, Y. Wang, A facile vapor–solid synthetic route to Sb_2O_3 fibrils and tubules, Chem. Phys. Lett. 363 (2002) 34–38.

[26] M. Hirasawa, T. Orii, T. Seto, Size-dependent crystallization of Si nanoparticles, Appl. Phys. Lett. 88 (2006) 093119.

[27] I.A. Degen, G.A. Newman, Raman spectra of inorganic ions, Spectrochim. Acta A: Mol. Spectrosc. 49 (1993) 859–887.

[28] J. Nayak, S.N. Sarangi, A.K. Dash, S.N. Sahu, Observation of semiconductor to insulator transition in Sb/Sb_2O_3 clusters synthesized by low-energy cluster beam deposition with different conditions, Vacuum 81 (2006) 366–372.

[29] D.W. Zeng, C.S. Xie, B.L. Zhu, W.L. Song, Characteristics of Sb_2O_3 nanoparticles synthesized from antimony by vapor condensation method, Mater. Lett. 58 (2004) 312–315.

[30] X. Ma, Z. Zhang, X. Li, Y. Du, F. Xu, Y. Qian, Micro-sized Sb_2O_3 octahedra fabricated via a PEG-1000 polymer-assisted hydrothermal route, J. Solid State Chem. 177 (2004) 3824–3829.

[31] Z. Deng, F. Tang, D. Chen, Z. Meng, L. Cao, B. Zou, A simple solution route to single-crystalline Sb_2O_3 nanowires with rectangular cross sections, J. Phys. Chem. B 110 (2006) 18225–18230.

[32] S. Fan, M.G. Chapline, N.R. Franklin, T.W. Tombler, A.M. Cassell, H. Dai, Self-oriented regular arrays of carbon nanotubes and their field emission properties, Science 283 (1999) 512–514.

[33] Z. Deng, D. Chen, F. Tang, X. Meng, J. Ren, L. Zhang, Orientated attachment assisted self-assembly of Sb_2O_3 nanorods and nanowires: end-to-end versus side-by-side, J. Phys. Chem. C 111 (2007) 5325–5330.

[34] S.H. Dalal, D.L. Baptista, K.B.K. Teo, R.G. Lacerda, D.A. Jefferson, W.I. Milne, Controllable growth of vertically aligned zinc oxide nanowires using vapour deposition, Nanotechnology 17 (2006) 4811–4818.

[35] F. Fang, D.X. Zhao, J.Y. Zhang, D.Z. Shen, Y.M. Lu, X.W. Fan, B.H. Li, X.H. Wang, The influence of growth temperature on ZnO nanowires, Mater. Lett. 62 (2008) 1092–1095.